Bistatic Radar Equation for Signals of Opportunity Revisited

Alexander G. Voronovich and Valery U. Zavorotny, *Fellow, IEEE*

***Abstract*— The bistatic radar equation currently used for simulating surface-reflected waveforms or delay-Doppler maps (DDMs), produced by signals of opportunity from global navigation satellites system (GNSS) or communication satellites, was previously derived under some limiting assumptions. One of them was the use of the Kirchhoff approximation in a geometric optics limit that assumes strong diffuse (noncoherent) scattering typical for very rough surfaces. This equation would produce an incorrect result for the case of weak diffuse scattering, or in the presence of coherent reflection. In this paper, it is shown that the assumption of strong diffuse scattering is not necessary in deriving such an equation. The derivation of a generalized bistatic radar equation is now based only on the assumption of roughness statistics being spatially homogeneous, and thus this equation is applicable for a much wider range of surface conditions and scattering geometries. This approach allows to correctly describe the transition from partially coherent scattering to completely noncoherent, strong diffuse scattering. It is demonstrated for the case of the GNSS-R DDMs simulated for a wide range of surface winds, and their transitional behavior is discussed.**

***Index Terms*— Electromagnetic scattering by rough surfaces, global positioning system (GPS), radar cross section, radar measurements, wind.**

I. Introduction

SIGNALS of opportunity, such as those generated by global navigation satellite system (GNSS) or by communication satellites, can be used for the Earth remote sensing purposes [1]–[8]. In [1], a bistatic radar equation was derived for simulating waveforms or delay-Doppler maps (DDMs) produced by the signals of global positioning system (GPS) reflected off the wind-roughened ocean surface. This equation was widely used for modeling of such GNSS reflections [5]. In deriving the bistatic radar equation, the authors followed the standard procedure based on a geometric optics limit of the Kirchhoff approximation. Besides that, it was assumed in that derivation that the regime of strong diffuse (noncoherent) scattering typical for rough surfaces takes place, which requires a large Rayleigh number, $R_a \gg 1$.

The radar equation would produce an incorrect result for the case of weak diffuse scattering or in the presence of coherent reflection. In this paper, we show that the assumption of strong diffuse scattering is not necessary in deriving such an equation. A generalized bistatic radar equation is systematically derived here from first principles. It consists of a sum of two terms, one for the coherent component and another for the noncoherent, diffuse component. The derivation of the generalized bistatic radar equation assumes only that surface roughness is statistically homogeneous and does not rely on any specific scattering model, and thus it is applicable for a wide range of surface conditions and scattering geometries. The part of the equation, which is responsible for noncoherent scattering, has the same structure as the old bistatic radar equation from [1]. The bistatic radar cross section (BRCS) entering the generalized radar equation does not necessarily obey the geometric optics approximation, and one can use any suitable scattering model for calculating the BRCS such as in [9]–[14].

Having the revisited bistatic radar equation in hand, one can correctly describe a transition from strong diffuse scattering to partially coherent scattering where the coherent component is present. This will be demonstrated here for the case of the ocean surface covered by wind-driven waves. If the rough ocean surface is such that $R_a \gg 1$, the scattered field will be due to the summation of a large number of uncorrelated quasi-specular surface reflections within a, so-called, glistening zone on the scattering surface. This regime is called strong diffuse scattering. However, if $R_a \lesssim 1$, a coherent component exists in a nominal specular direction superimposed with a weak diffuse "halo." This case is not accounted for by the radar equation in [1].

Partially coherent scattering in the near-forward bistatic geometry drew the attention of researchers long ago, and various scattering models were proposed [4], [15], [16]. The importance of the accounting for the coherent component in near-nadir scattering for ice altimetry was first stressed in [17]. The presence of the coherent component was reported both in ice altimetry data [18] and ocean altimetry data [19]. The numerical model for partially coherent bistatic scattering of GNSS-type signals from the land with vegetation was developed in [20]–[22]. Frequently, it is found convenient incorporating the specular, coherent component into the bistatic radar equation in the form of a so-called coherent BRCS added to a diffuse BRCS and placed under the integral over a scattering surface [4]. This type of BRCS is known in the literature as a near-field radar cross section [23], [24]. Generally, the coherent BRCS includes a sharp finite-support function having a peak in a specular direction and describing an EM wave diffraction on a finite area of interest, multiplied by the factor that accounts for a reflection coefficient, an antenna pattern, and distance. In contrast to the coherent

Manuscript received April 12, 2017; revised August 8, 2017 and October 13, 2017; accepted October 26, 2017. Date of publication December 4, 2017; date of current version March 23, 2018. *(Corresponding author: Valery U. Zavorotny.)*

The authors are with the Earth System Research Laboratory, National Oceanic and Atmospheric Administration, Boulder, CO 80305 USA (e-mail: alexander.voronovich@noaa.gov; valery.zavorotny@noaa.gov).

Digital Object Identifier 10.1109/TGRS.2017.2771253

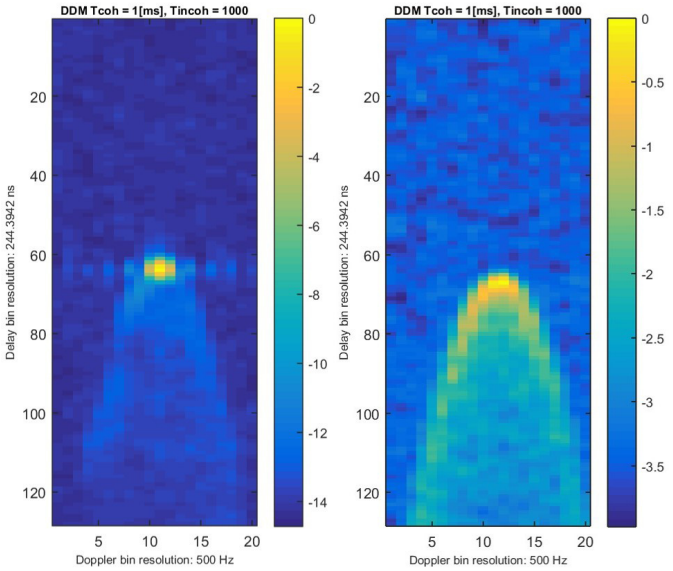

Fig. 1. Example of the DDMs obtained during the UK TDS-1 satellite mission [26]. (Left) DDM showing the presence of coherent (specular) reflection. (Right) DDM obtained under the conditions of strong noncoherent (diffuse) scattering. Color bar is in decibels.

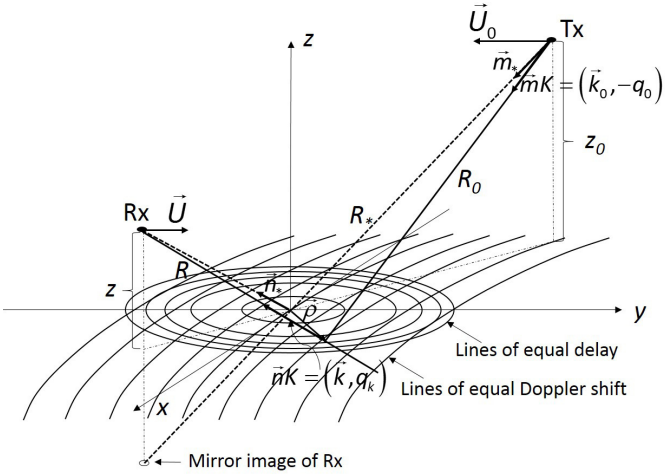

Fig. 2. Scattering geometry of the problem.

BRCS, the diffuse BRCS represents a traditional far-field radar cross section being a characteristic of the scattering object alone, and not a function of the radar system or the distance between radar and the scattering object [25].

To the best of our knowledge, the first coherent GNSS reflected signals observed from space, along with more common diffusive scattered GNSS signals, were recorded during the mission of the U.K. TDS-1 satellite. These two regimes can be clearly seen while analyzing DDMs obtained with the TDS-1 satellite.

Fig. 1 gives the examples of such DDMs [26]. Fig. 1 (right) shows the DDM at a fully diffuse scattering regime from a rough ocean surface with a large R_a. The DDM has a characteristic horseshoe shape. Fig. 1 (left) shows the DDM obtained in the presence of the first-year ice in the antenna footprint. Because the first-year ice is significantly lesser rough than the ocean surface with wind waves, an additional feature emerges in the DDM, which is located at a specular delay and stretched horizontally, along the Doppler frequency axis. This feature corresponds to a coherent reflection event. The rest is due to diffuse scattering, possibly from both rough ice and the wavy ocean surface.

Additionally, we present one more modification to the bistatic radar equation. It pertains to the Doppler effect due to the motion of both the GNSS transmitter and the receiver with respect to the envelope of the signal. Recently, a similar kinematic effect on the envelope of the direct GNSS signal was discussed in [27] and [28]. In [1], only the Doppler effect of changing the carrier frequency of the reflected signal was considered. While the Doppler effect on the signal envelope is not significant when using airborne GNSS bistatic radars, potentially it can be noticeable in altimetric measurements from low-Earth orbit platforms at incidence angles significantly deviating from nadir. Such a geometry was proposed for prospective GNSS space-borne wide-swath altimetry [29]–[31]. The corresponding kinematic effect could diminish the accuracy of such altimetric measurements at incidence angles significantly deviating from nadir. The improved version of the bistatic radar equation presented here allows accounting for such an effect.

II. Problem Formulation

In [1], the theoretical model for calculation of the DDMs for GPS signals reflected/scattered from a rough sea surface was proposed. Let us summarize the basic concept of the technique and scattering geometry (see Fig. 2) to be considered. The DDM follows after squaring and averaging the processed signal, which is a cross correlation of the received signal envelope $\widetilde{\Psi}_{sc}$ with the replica of the transmitted signal envelope $a(t)$

$$Y(t,\tau,\omega_D)=\frac{1}{T_i}\int_0^{T_i}\widetilde{\Psi}_{sc}(t+t')a^*(t+t'-\tau)e^{i\omega_D t'}dt' \tag{1}$$

where t is a running time, τ and ω_D are, respectively, a time delay and a frequency offset aimed to compensate a possible Doppler shift of the signal, and T_i is a coherent integration time. By changing both τ and ω_D, one can create a 2-D DDM. By fixing one of those two parameters and varying another, the DDM turns into a 1-D delay, or Doppler frequency, waveform. Historically, the first measurements of GPS reflected signals were performed by obtaining the delay waveforms [32]. In the general case, processed signal $Y(t,\tau,\omega_D)$ includes both coherent and noncoherent components. In [1], the coherent component was not included into consideration, since in the typical cases of moderate or strong winds it is negligible. However, in certain situations associated with low wind or scattering from relatively flat areas such as young sea ice or lakes, it may become significant. Here, the general case is considered where both components may be present simultaneously.

A detailed derivation of the generalized version of the DDM bistatic radar equation is presented in the Appendix. For the purpose of current consideration, we summarize the results by

referring to (A34) and (A45), which are the two terms of the DDM general expression. It reads

$$\overline{|Y(\tau,\omega_D)|^2} = \overline{|Y(\tau,\omega_D)|_c^2} + \overline{|Y(\tau,\omega_D)|_{nc}^2}. \tag{2}$$

Here, the contribution from the coherent component is as follows:

$$\overline{|Y(\tau,\omega_D)|_c^2} = P_{\rm tr}|D_{\rm tr}(\vec{n}_*,\omega_0)D_{\rm rec}(\vec{m}_*,\omega_0)|^2 \times \left\langle \left| \chi\left(\tau - \frac{R_*}{c}, \delta\omega_*, \beta_*\right)\right|^2 \right\rangle \frac{|\overline{V}(\vec{n}_{*\perp},\omega_0)|^2}{R_*^2} \tag{3}$$

where

$$\delta\omega_* = \Delta\omega_* - \omega_D; \quad \Delta\omega_* = \frac{\omega_0}{c}(\vec{m}_*\vec{U}_0 - \vec{n}_*\vec{U}) \tag{4}$$

$$\beta_* = 1 - \frac{\Delta\omega_*}{\omega_0}. \tag{5}$$

The following notations are used here and in the following: the subscript (*) indicates that the corresponding parameters are associated with the coherent component, ω_0 is a central frequency of the transmitted signal, which is supposed to be narrow band, $P_{\rm tr}$ is a transmitter power, $(\vec{r}_0, z_0)$ and $(\vec{r}, z)$ are the horizontal and vertical coordinates of the transmitter and the receiver, correspondingly (the z-axis is directed upward), $D_{\rm tr}$ and $D_{\rm rec}$ are, respectively, the transmitter and receiver antenna directivity factors (voltage units), R_* is a distance between the transmitter and the specular image of the receiver:

$$R_* = \sqrt{(\vec{r} - \vec{r}_0)^2 + (z + z_0)^2} \tag{6}$$

$\vec{m}_*$ is a unit vector directed from the transmitter toward the specular image of the receiver

$$\vec{m}_* = (\vec{m}_{*\perp}, m_{*z}) = \frac{1}{R_*}(\vec{r} - \vec{r}_0, -z - z_0) \tag{7}$$

$\vec{n}_*$ is a unit vector directed from the specular image of the transmitter toward the receiver

$$\vec{n}_* = (\vec{n}_{*\perp}, n_{*z}) = \frac{1}{R_*}(\vec{r} - \vec{r}_0, z + z_0) \tag{8}$$

$\vec{U}_0 = (\vec{u}^0, u_z^0)$ and $\vec{U} = (\vec{u}, u_z)$ are the velocity vectors of the transmitter and the receiver, correspondingly, and $\chi(\delta\tau, \delta\omega_*, \beta_*)$ is the so-called Woodward ambiguity function (WAF), which is a modification of the WAF used in [1] due to an extra parameter β_* describing the Doppler effect with respect to the signal envelope

$$\chi(t, \delta\tau, \delta\omega_*, \beta_*) = \frac{1}{T_i}\int_t^{T_i+t} a(\beta_* t' + \delta\tau)a^*(t')e^{-i\delta\omega_* t'}dt'. \tag{9}$$

The details of related derivations can be found in the Appendix. The function χ in (9), generally, depends on time t. In practice, the ensemble averaging referred in (2) by the overbar is performed as an averaging over the observation time T, which is much larger than the coherent integration time T_i. In this case, averaging with respect to statistically independent realizations of both roughness and transmitted pulses is, in fact, made simultaneously. For this reason, the expression in angular brackets in (3) has the following meaning:

$$\langle|\chi(\delta\tau, \delta\omega_*, \beta_*)|^2\rangle = \lim_{T\to\infty}\frac{1}{2T}\int_{-T}^{T}|\chi(t, \delta\tau, \delta\omega_*, \beta_*)|^2 dt. \tag{10}$$

Assuming that ω_D is selected such that the Doppler shift is exactly compensated in the carrier so that $\delta\omega_*$ in (4) turns to zero, then WAF in (3) turns into autocorrelation function of the transmitted signal, and the coherent part of the waveform $\overline{|Y(\tau,\omega_D)|_c^2}$ becomes equal to this autocorrelation function multiplied by the corresponding spherical spread and reflection factors, $1/R_*^2$ and $|\overline{V}(\vec{n}_{*\perp},\omega_0)|^2$, where $\overline{V}(\vec{n}_{*\perp},\omega_0)$ is an average reflection coefficient calculated in a direction $\vec{n}_{*\perp}$. One can see that (3) corresponds to the case of a perfectly flat surface if one replaces average reflection coefficient $\overline{V}$ by the corresponding Fresnel reflection coefficient.

In the case of Gaussian statistics of roughness factor, $|\overline{V}(\vec{n}_{*\perp},\omega_0)|^2$ with a good accuracy can be expressed via the Fresnel reflection coefficient V_F of the underlying medium [14]

$$|\overline{V}(\vec{n}_{*\perp},\omega_0)|^2 = \exp\left(-4R_a^2\right)|V_F(\vec{n}_{*\perp},\omega_0)|^2 \tag{11}$$

where

$$R_a = \frac{\omega_0}{c}n_{*z}\langle h^2\rangle^{1/2} \tag{12}$$

is a Rayleigh roughness parameter, and n_{*z} is the vertical component of vector $\vec{n}_*$ defined in (8).

Now, we turn to the expression for the noncoherent component of the waveform in (2)

$$\overline{|Y(\tau,\omega_0)|_{nc}^2} = \frac{P_{\rm tr}}{4\pi}\int\int\frac{|D_{\rm tr}(\vec{m}_\perp,\omega_0)D_{\rm rec}(\vec{n}_\perp,\omega_0)|^2}{R_0^2R^2} \times \left\langle\left|\chi\left(\beta\tau - \frac{R_0+R}{c}, \delta\omega, \beta\right)\right|^2\right\rangle \sigma_0(\vec{n}_\perp, \vec{m}_\perp; \omega_0)d\vec{\rho}. \tag{13}$$

Here, the integration proceeds over the scattering plane surface with $\vec{\rho}$ being a position of the scattering element on this surface; $\vec{m}$ and $\vec{n}$ are, respectively, the 3-D vectors pointing from the transmitter to the scattering element on the surface

$$\vec{m} = (\vec{m}_\perp, m_z) = \frac{1}{R_0}(\vec{\rho} - \vec{r}_0, -z_0) \tag{14}$$

and from the scattering element on the surface to the receiver

$$\vec{n} = (\vec{n}_\perp, n_z) = \frac{1}{R}(\vec{r} - \vec{\rho}, z) \tag{15}$$

R_0 and R are the distances between the scattering element and the transmitter and the receiver, correspondingly

$$R_0 = \sqrt{(\vec{\rho} - \vec{r}_0)^2 + z_0^2}, \quad R = \sqrt{(\vec{r} - \vec{\rho})^2 + z^2} \tag{16}$$

$\delta\omega$ is a corresponding Doppler shift similar to (4); however, now it is associated with an arbitrary scattering element on

the rough surface rather than with a nominal specular point on the mean-level surface

$$\delta\omega = \Delta\omega - \omega_D; \quad \Delta\omega = \frac{\omega_0}{c}(\vec{m}\vec{U}_0 - \vec{n}\vec{U}) \tag{17}$$

and

$$\beta = 1 - \frac{\Delta\omega}{\omega_0}. \tag{18}$$

It is clear that parameter $\Delta\omega$ describes both a Doppler effect pertaining to the carrier of the scattered signal and a Doppler effect with respect to the envelope of the signal. It is determined by the difference between radial components of the transmitter and receiver velocities.

In (13), $\sigma_0(\vec{n}_\perp, \vec{m}_\perp, \omega_0)$ is a bistatic scattering cross section per unit area (a dimensionless value) with $\vec{m}_\perp = (\vec{\rho} - \vec{r}_0)/R_0$, $\vec{n}_\perp = (\vec{r} - \vec{\rho})/R$ being horizontal components of the incident and scattered wave vectors, respectively. Physical meaning of (13) is quite straightforward: each surface scattering element contributes to the average waveform with time delay $\delta\tau$ and Doppler shift $\delta\omega$ and with weight proportional to the bistatic scattering cross section σ_0. Factors R_0^{-2} and R^{-2} account for spherical propagation to and from the scattering element. All these parameters depend on the location $\vec{\rho}$ of the scattering element.

In a strong diffuse regime, when $R_a \gg 1$ and the geometric optics approximation can be applied for calculations of σ_0, one obtains an explicit analytical expression for the bistatic scattering cross section

$$\sigma_0(\vec{n}_\perp, \vec{m}_\perp; \omega_0) = \pi \left| V_F\left(\frac{\vec{n}_\perp + \vec{m}_\perp}{2}, \omega_0\right)\right|^2 \times \left(1 + \left|\frac{\vec{n}_\perp - \vec{m}_\perp}{n_z + m_z}\right|^2\right) P\left(-\frac{\vec{n}_\perp - \vec{m}_\perp}{n_z + m_z}\right) \tag{19}$$

where P is a probability density function of surface slopes [1].

In the previous model [1], only the Doppler effect of changing the carrier frequency of the reflected signal due to the motion of both the GNSS transmitter and the receiver was accounted, whereas a similar effect with respect to the envelope of the signal was deemed negligible. The proposed model for the WAF accounts for this effect by introducing the parameter β.

Let us consider the correction to the WAF associated with β_* which with good accuracy also applies for the case of β. It should be stressed here that the analogous Doppler effect influences also the WAF of the direct signal due to a relative motion of both the transmitter and the receiver [27], [28]. According to (9) and (18), over the time period T_i, the correction term will produce a negligible shift in the argument of the envelope function a provided

$$T_i \Delta f \frac{U_r}{c} \ll 1 \tag{20}$$

where Δf is the signal bandwidth, and $\Delta U_r = \vec{m}_*\vec{U}_0 - \vec{n}_*\vec{U}$ is a difference of the radial velocities of the transmitter and the receiver. In the case of GPS (C/A-code) signals, $\Delta f \approx 10^6$ Hz, and usually $T_i \sim 10^{-3}$ s. For incidence close to nadir, U_r/c is negligibly small, but at grazing angles and for the low-Earth orbit receiving satellite, $U_r/c \approx 2 \cdot 10^{-5}$, which gives for $T_i \Delta f U/c \approx 2 \cdot 10^{-2}$. Therefore, for all range of incidence angles, one can consider the condition (20) fulfilled and approximation $\beta = 1$ justified. This condition would work for current GNSS-R applications. In this case, with high accuracy, β can be set to 1, and (9) reduces to the standard definition of the WAF. However, in the case of GPS [P(Y)-code, or similar] signals with $\Delta f \approx 10^7$ Hz, the left-hand side of (20) increases to 0.2, which might require using a more accurate expression for the WAF with $\beta \neq 1$. Recently, GNSS-R altimetric technique was proposed, which is using large incidence angles to provide wide-swath performance [29]–[31]. The above-discussed Doppler effect with respect to the WAF could degrade the anticipated 5-cm accuracy of altimetric measurements with a proposed instrument, which should provide multifrequency observations to correct for the ionospheric delay [33].

Equations (3) and (13) were derived assuming a plane (on average) scattering surface. If, however, the mean curvature of this surface needs to be taken into account, one can still use these equations. In this case, in (3), one has to use the values $\vec{m}_{*\perp}$ and $\vec{n}_{*\perp}$ that correspond to the nominal specular point, and in (13), one has to integrate over a curved surface, substituting $\vec{m}_\perp$, $\vec{n}_\perp$, and so on for values that lie in the plane tangent to the surface at the integration point $\vec{\rho}$.

The formulation considered in this section may be applied not only to GNSS signals but also to any point-like source of opportunity (e.g., communication satellites or satellite radio) with the only difference being that the envelope $a(t)$ is not known in advance. In this case, the reflected signal can be cross correlated with the direct signal itself after proper Doppler frequency and delay adjustments similar to what was suggested in the so-called interferometric GNSS-R processing [33]. The Doppler effect associated with the envelope of the signal can be of some significance for sources of opportunity with larger then considered above bandwidths Δf or integration times T_i.

III. Simulation of Delay-Doppler Maps

In what follows, (2), (3), and (13) and the scattering models based on the small-slope approximation (SSA) from [14] and [35] for calculating σ_0 were incorporated into the code that generated DDMs for a range of winds and the specific geometry and receiver parameters, so the transition from weak to moderate winds can be studied. In these calculations, we assume $\beta = 1$.

To perform calculations, one has to specify an expression for the WAF, which enters (3) and (13). Here, we use the following approximate expression for the absolute-value squared WAF, which was suggested in [1] for GPS application:

$$\langle|\chi(\delta\tau, \delta\omega)|^2\rangle = \Lambda^2(\delta\tau)\left(\frac{\sin(\delta\omega T_i/2)}{\delta\omega T_i/2}\right)^2 \tag{21}$$

with

$$\Lambda(\delta\tau) = \begin{cases} 1 - |\delta\tau|/\tau_c, & |\delta\tau| \le \tau_c \\ 0, & |\delta\tau| > \tau_c \end{cases} \tag{22}$$

where τ_c is the chip length. This factorization of the WAF appeared to work quite well. Our calculations of the exact

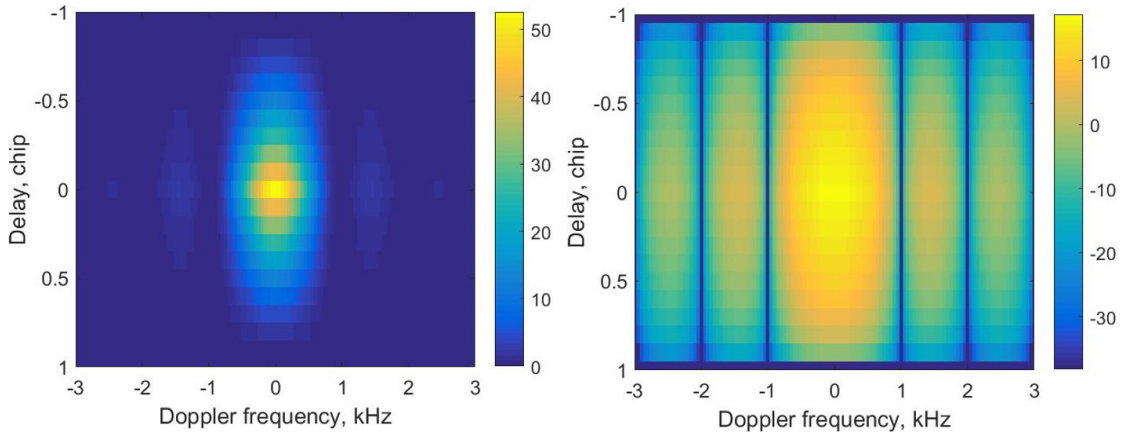

Fig. 3. Simulated coherent component of the DDM in the regime of weak diffuse scattering at $U = 2$ m/s. (Left) Linear scale. (Right) To make sidelobes more visible (in decibels).

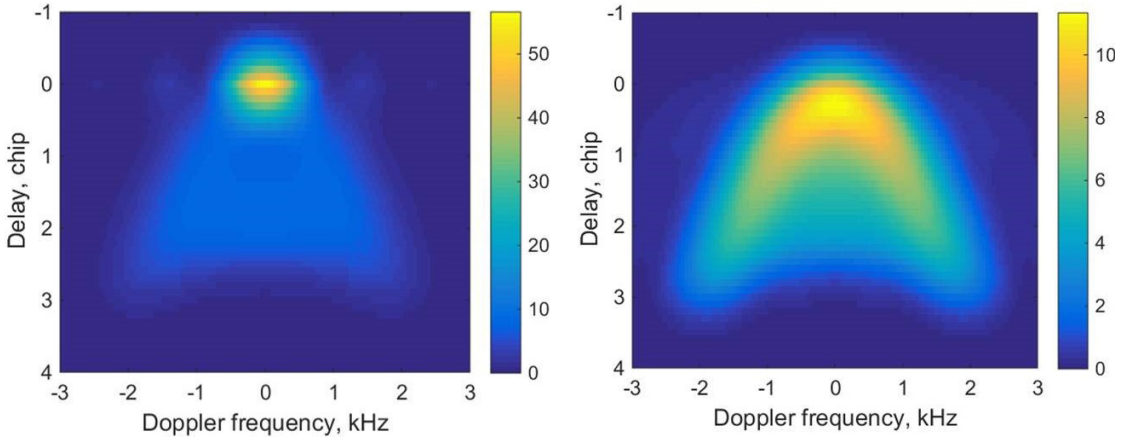

Fig. 4. Simulated DDM (linear scale) that combines coherent and diffusive components for (Left) $U = 2$ m/s (the same regime as in Fig. 2) and (Right) $U = 3$ m/s (coherent component diminishes significantly).

and approximate expressions for WAF demonstrate up to 10^{-4} relative accuracy for the factorization. In the case of $\beta \neq 1$, it is not possible to obtain an analytical expression similar to (21), but the numerical simulations show that the factorization of the WAF also holds with high enough accuracy in the following form:

$$\langle |\chi(\delta\tau, \delta\omega; \beta)|^2 \rangle = \langle |\chi(\delta\tau, 0; \beta)|^2 \rangle \cdot \langle |\chi(0, \delta\omega; \beta)|^2 \rangle. \quad (23)$$

First, we would like to show how the simulated DDM behaves for the case of weak winds when a strong coherent component manifests itself. Fig. 3 shows a simulation of the DDM originated from a reflected GPS L1 signal seen at the incidence angle of 30° for the receiver altitude of 5 km with the circular antenna having 14-dB directivity, which translates into ~40° wide main lobe pointed into a specular direction. For calculation of the Rayleigh parameter R_a, the ocean surface roughness was assumed obeying the Elfouhaily *et al.* [36] wave spectral model. For this case, wind speed was chosen $U_{10} = 2$ m/s, which yields $R_a = 0.71$. The coherent DDM has a strong central lobe and much weaker sidelobes mirroring the structure of the WAF of the GPS signal [1], [2]. These sidelobes are barely seen in Fig. 3 (left) because of the linear scale for the DDM power chosen here. To better see the sidelobes of the coherent DDM, we plot the same image in the dB scale in Fig. 3 (right).

Fig. 4 (left) shows a DDM, which combines together both the coherent and diffuse components for the case of $U_{10} = 2$ m/s. The geometry and receiver parameters were chosen the same as for the case shown in Fig. 3. It is seen that the coherent component dominates the DDM. The case of $U_{10} = 3$ m/s is shown in Fig. 4 (right). The coherent component is less pronounced, while the diffuse component is relatively stronger, although both components reduce in a magnitude due to the increased surface roughness.

To compare DDMs for a wider range of winds (between 2 and 5 m/s), we plotted a set of waveforms or 1-D cuts of the DDMs at the zero Doppler frequency. They are shown in Fig. 5. One can see that a significant reduction of the peak of the waveforms takes place between 2 and 3 m/s. It happens mostly because of the fast decay of the coherent component due to its exponential dependence on R_a^2 [see (11)]. Note that the waveforms at $U_{10} > 3$ m/s produced by the weak diffuse scattering are vanishing at about three-chip delay. This is a result of the limited footprint created by the 40° wide beam of the antenna located at $H = 5$ km. Such set of parameters was chosen to reduce the computation time of the DDMs.

In addition, simulations of the DDM were performed using the geometric optics model [1] based on a large R_a assumption (fully diffuse scattering) for a large range of winds from 2 to 25 m/s. A comparison between these results and those

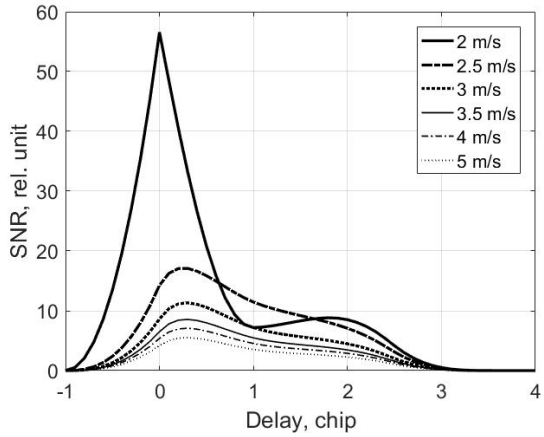

Fig. 5. Transition from coherent reflection at $U = 2$ m/s to weak diffuse noncoherent scattering at $U = 2.5$–5 m/s.

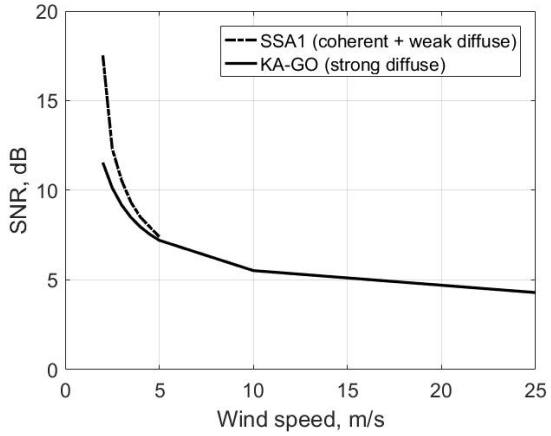

Fig. 6. DDM peak SNR as a function of wind speed. Comparison between coherent + weak diffuse and strong diffuse scattering.

obtained with the partially coherent model [14] shows that a smooth transition from one to another takes place at $U_{10} \approx 5$ m/s. At $U_{10} < 5$ m/s, the model [1] inaccurately predicts the behavior of DDM giving lower values compared to the results following from the more accurate model [14] based on a partially coherent, weakly diffuse scattering process. This is shown in Fig. 6.

IV. Conclusion

The bistatic radar equation that was derived in [1] for simulating DDMs, or waveforms produced by GPS signals reflected off the rough ocean surface cannot be applied to the case of weak diffuse scattering or in a presence of coherent reflection. In deriving that equation, a geometric optics limit of the Kirchhoff approximation under the regime of strong diffuse (noncoherent) scattering with $R_a \gg 1$ was used.

Sometimes, however, a weak diffuse scattering scenario takes place. It might be seen in bistatic scattering from calm seas, lakes, relatively flat land, or sea ice characterized by small R_a. In this paper, it was shown that the assumption of strong diffuse scattering is not necessary in deriving such an equation. The generalized bistatic radar equation was derived here using a formalism of scattering amplitudes. Now, this equation consists of a sum of two terms, one for the coherent component and another for the noncoherent, diffuse component. This bistatic radar equation is applicable for a much wider range of surface conditions and scattering geometries. The part of the equation, which describes noncoherent diffuse scattering, has the same structure as the old bistatic radar equation from [1]. However, the BRCS σ_0 entering this new, generalized equation does not necessarily need to obey the geometric optics approximation (19). It can originate from an arbitrary scattering model.

Using the generalized bistatic radar equation, we simulated a set of DDMs in order to illustrate a transition from strong diffuse scattering to partially coherent scattering, and then, to the emergence of the coherent component. This was demonstrated for the case of the ocean surface covered by wind-driven waves. The DDMs at the regime of weak winds, when $R_a < 1$, were simulated using the SSA1 approximation for calculating σ_0, which cannot be correctly described by the probability density function of surface slopes according to (19). It is shown that for scattering from surfaces with a small enough Rayleigh parameter, a coherent component which manifests itself only at a nominal specular direction might contribute noticeably to the peak value of the DDM. It is accompanied by a relatively weak diffuse scattering away from the DDM peak. Because coherent and noncoherent scattering components have a different nature and obey different dependences on the problem geometry, the relative weight of corresponding components in DDMs varies depending on a problem specific setup.

The presence of the coherent component in the DDM needs special attention when using it for both altimetry and scatterometry purposes. The leading slope and peak positions of the reflected waveform for the diffuse incoherent component are somewhat delayed with respect to those for the coherent component. If the coherent scattering is mistakenly interpreted as incoherent diffuse scattering, the modeling result will produce a positive bias in the surface level prediction. This bias can be estimated using our revisited radar equation if information about surface roughness (Rayleigh parameter and mean square slope) is available. The new bistatic radar model also addresses the issue of kinematic effects influencing the WAF that becomes important for GNSS-R altimetry at incidence angles significantly deviating from nadir.

Eight microsatellites have been launched on December 15, 2016 as a part of the NASA mission called the Cyclone Global Navigation Satellite System (CYGNSS). This is the first mission dedicated to retrieve ocean winds and waves in tropical cyclones using GNSS signals [7]. To simulate the performance of the onboard DDM receiver under these conditions, an end-to-end simulator (E2ES) was designed [37], which employs the DDM bistatic radar equation based on the strongly diffuse scattering model from [1]. This simulator was used for an assessment of both the diffuse BRCS and wind retrieval algorithms for the CYGNSS mission [38]–[40]. The generalized bistatic radar equation presented here can be used to augment the E2ES simulator with an ability to correctly predict the DDM behavior also for the ocean surface under weak winds characterized by relatively low values of the Rayleigh parameter R_a.

APPENDIX
DERIVATION OF THE BISTATIC RADAR EQUATION

Let us first outline seven principal steps of the derivation of the bistatic radar equation. Those are: 1) representation of the incident field in (A5) as a superposition of plane waves with different frequencies and projections of the horizontal wave vectors (i.e., incidence angles); 2) expressing the scattered field for each incident plane wave using a scattering amplitude [see (A6)]; 3) obtaining expression (A7) for the scattered field using the principle of superposition, and writing it down for the case of a moving transmitter and receiver [see (A10)]; 4) integrating (A10) over the frequency and producing expression (A14) for the waveform; 5) obtaining simplified expression (A21) for the average square of the waveform using a far-field assumption (A20); 6) averaging an absolute-value square of the waveform with respect to realizations of statistically spatially homogeneous roughness using (A22), which leads to appearance of both coherent and noncoherent components of the waveform [see (A24)]; and 7) obtaining the expressions (A34) and (A45) in a final form for, respectively, coherent and noncoherent components.

All derivations in the following are performed for a scalar field assuming that we are dealing with the waves of a certain polarization. The general case would only require the introduction of corresponding polarization indices into the scattering amplitude $S(\vec{k},\vec{k}_0)$ [34]. To simplify notations without loss of generality, we omit polarization indexes in $S(\vec{k},\vec{k}_0)$ in what follows.

A well-known plane-wave representation of the field radiated by an omnidirectional point source located at a point with horizontal and vertical coordinates, $\vec{r}_0$ and $z_0 > 0$, respectively, reads

$$\frac{e^{i(\omega/c)R}}{R} = \frac{i}{2\pi}\int \frac{d\vec{k}}{q_k} e^{i\vec{k}(\vec{r}-\vec{r}_0)+iq_k(z_0-z)} \tag{A1}$$

where

$$R = \sqrt{(\vec{r}-\vec{r}_0)^2+(z-z_0)^2} \tag{A2}$$

and

$$q_k = \sqrt{\frac{\omega^2}{c^2}-k^2} \tag{A3}$$

is a vertical component of the wave vector with horizontal component $\vec{k}$. It is assumed in (A1) that $z_0 > z$ (the receiving point is below the source). If we want to describe a directional source, the integral in (A1) can be modified by including a directivity factor $D_{\rm tr}(\vec{k})$ under its sign. In the far field, $R \to \infty$, such an integral can be evaluated by the steepest descent method and the result reads

$$\frac{i}{2\pi}\int \frac{d\vec{k}}{q_k} D_{\rm tr}(\vec{k}) e^{i\vec{k}(\vec{r}-\vec{r}_0)+iq_k(z_0-z)} \approx D_{\rm tr}\left(\frac{\omega}{c}\frac{\vec{r}-\vec{r}_0}{R}\right)\frac{e^{i(\omega/c)R}}{R}. \tag{A4}$$

Thus, the field $\Psi_{\rm in}$ incident upon the sea surface due to a source with a transmitter power $P_{\rm tr}$ and an antenna directivity $D_{\rm tr}(\vec{k})$ can be represented as follows:

$$\Psi_{\rm in}(\vec{r},z) = \frac{i}{2\pi}\sqrt{P_{\rm tr}}\int d\vec{k}_0 D_{\rm tr}(\vec{k}_0)\frac{1}{q_{k_0}^{1/2}} e^{-i\vec{k}_0\vec{r}_0+iq_{k_0}z_0} \times \frac{1}{q_{k_0}^{1/2}} e^{i\vec{k}_0\vec{r}-iq_{k_0}z} \tag{A5}$$

where we replaced integration variable $\vec{k}$ by $\vec{k}_0$. The last factor in (A5) represents an individual plane wave propagating downward. In the general case, the scattered field due to such a single incident plane wave can be expressed in terms of scattering amplitude $S(\vec{k},\vec{k}_0)$ [34]

$$\psi_{sc}(\vec{r},z) = \int d\vec{k}\frac{1}{q_k^{1/2}} e^{i\vec{k}\vec{r}+iq_kz} S(\vec{k},\vec{k}_0) \tag{A6}$$

(the scattered waves propagate upward). Using a superposition principle, one can express the scattered field due to $\Psi_{\rm in}$ in (A5)

$$\Psi_{sc}(\vec{r},z) = \frac{i}{2\pi}\sqrt{P_{\rm tr}}\int d\vec{k}_0 D_{\rm tr}(\vec{k}_0)\frac{1}{q_{k_0}^{1/2}} e^{-i\vec{k}_0\vec{r}_0+iq_{k_0}z_0} \times \int d\vec{k} D_{\rm rec}(\vec{k})\frac{1}{q_k^{1/2}} e^{i\vec{k}\vec{r}+iq_kz} S(\vec{k},\vec{k}_0). \tag{A7}$$

Here, similar to (A4), we also introduced an antenna directivity factor for the receiver $D_{\rm rec}(\vec{k})$.

Let the transmitter radiate a narrow-band signal with envelope $a(t)$ and central frequency ω_0

$$a(t)e^{-i\omega_0 t} = \int \widehat{a}(\omega)e^{-i\omega t}d\omega \tag{A8}$$

where signal spectrum $\widehat{a}(\omega)$ is concentrated in the vicinity of ω_0. The temporal dependence of the scattered signal can be derived from (A7) after additional integration with respect to frequency ω. Note that both q_{k_0} and q_k are the functions of the frequency [see (A3)]; although to simplify the notations in the following, we will not indicate this dependence explicitly. If, besides that, both the transmitter and the receiver move with nonrelativistic velocities, this motion can be accounted for by making a substitution

$$\vec{r}_0 \to \vec{r}_0 + \vec{u}^{(0)}t, \quad z_0 \to z_0 + u_z^{(0)}t \tag{A9}$$

in (A7), and, similarly, for $(\vec{r},z)$. Now, $\vec{r}_0$, $\vec{r}$, z_0, and z stand for the coordinates of the transmitter and the receiver at $t=0$; $\vec{u}^{(0)}$ and $\vec{u}$ stand for horizontal and $u_z^{(0)}$ and u_z for the vertical components of the transmitter and receiver velocity vectors, respectively. The resulting expression for the envelope of the received field $\widetilde{\Psi}_{sc}$ as a function of time reads

$$\begin{aligned}\widetilde{\Psi}_{sc}(t) &= \Psi_{sc}(t)e^{-i\omega_0 t} \\ &= \frac{i\sqrt{P_{\rm tr}}}{2\pi}\int \widehat{a}(\omega)d\omega \int \frac{d\vec{k}_0}{q_{k_0}^{1/2}} D_{\rm tr}(\vec{k}_0)\int \frac{d\vec{k}}{q_k^{1/2}} D_{\rm rec}(\vec{k}) \\ &\quad \times S(\vec{k},\vec{k}_0)e^{i\vec{k}\vec{r}-i\vec{k}_0\vec{r}_0+iq_kz+iq_{k_0}z_0-i\Omega t}\end{aligned} \tag{A10}$$

where

$$\Omega = \omega - \omega_0 + \vec{k}_0\vec{u}_0 - q_{k_0}u_z^{(0)} - \vec{k}\vec{u} - q_ku_z.$$

The next step is to perform integration in (A10) over frequency ω. To be able to do this, we consolidate the frequency

dependence in the exponent in the form of a linear function of ω by rescaling our integration variables $\vec{k}$ and $\vec{k}_0$ by ω. Functions $D_{\rm tr}$, $D_{\rm rec}$, and S are the slow functions of ω as compared to the fast oscillating phase term. For this reason, we can set $\omega = \omega_0$ in those functions. Now, using (A8), we can integrate over frequency and obtain

$$\widetilde{\Psi}_{sc}(t) = \frac{i\sqrt{P_{\rm tr}}}{2\pi}\int D_{\rm tr}(\vec{k})D_{\rm rec}(\vec{k}_0)S(\vec{k},\vec{k}_0) \times \exp\left[i\omega_0\tau_0(\vec{k},\vec{k}_0) + i\,\Delta\omega(\vec{k},\vec{k}_0)t\right] \times a[(1-\Delta\omega(\vec{k},\vec{k}_0)/\omega_0)t - \tau_0(\vec{k},\vec{k}_0)]\frac{d\vec{k}d\vec{k}_0}{\sqrt{q_k q_{k_0}}} \tag{A11}$$

where

$$\Delta\omega(\vec{k},\vec{k}_0) = \vec{k}\vec{u} + q_k u_z - \vec{k}_0\vec{u}^{(0)} + q_{k_0}u_z^{(0)} \tag{A12}$$

$$\tau_0(\vec{k},\vec{k}_0) = \frac{\vec{k}\vec{r} + q_k z - \vec{k}_0\vec{r}_0 + q_{k_0}z_0}{\omega_0} \tag{A13}$$

and q_k and q_{k_0} are calculated at $\omega = \omega_0$.

Substituting (A11) into (1) and using (9) for the WAF, we obtain

$$Y(t,\tau,\omega_D) = \frac{i\sqrt{P_{\rm tr}}}{2\pi}e^{-i\omega_D t - i\delta\omega\tau}\int\int D_{\rm tr}(\vec{k}_0)D_{\rm rec}(\vec{k}) \times S(\vec{k},\vec{k}_0)\exp[i\omega_0\tau_0(\vec{k},\vec{k}_0)] \times \chi(t-\tau,\delta\tau,\delta\omega,\beta)\frac{d\vec{k}_0 d\vec{k}}{\sqrt{q_k q_{k_0}}} \tag{A14}$$

where

$$\delta\tau = \beta\tau - \tau_0 \tag{A15}$$

$$\delta\omega = -\Delta\omega - \omega_D \tag{A16}$$

$$\beta = 1 - \frac{\Delta\omega}{\omega_0}. \tag{A17}$$

Parameter β takes into account Doppler effect with respect to the envelope of the transmitted signal. Note that parameters $\delta\tau$, $\delta\omega$, and β depend on $\vec{k}$ and $\vec{k}_0$; to simplify the notation, we do not indicate this in (A14) explicitly.

Now, let us consider $|Y(\tau,\omega_D)|^2$ and average this value with respect to statistical ensemble of roughness assuming the latter being statistically homogeneous with respect to horizontal coordinates. To do this, we square (A14) denoting integration variables $\vec{k}_0$ and $\vec{k}$ as $\vec{\kappa}_0'$ and $\vec{\kappa}'$ and $\vec{\kappa}_0''$ and $\vec{\kappa}''$, respectively, and then introduce new integration variables $\vec{k}_0$, $\vec{k}$, $\vec{b}$, and $\vec{b}_0$ as follows:

$$\vec{\kappa}_0' = \vec{k}_0 - \frac{\vec{b}_0}{2},\quad \vec{\kappa}_0'' = \vec{k}_0 + \frac{\vec{b}_0}{2},\quad \vec{\kappa}' = \vec{k} - \frac{\vec{b}}{2},\quad \vec{\kappa}'' = \vec{k} + \frac{\vec{b}}{2}. \tag{A18}$$

Statistics of roughness enters (A14) through scattering amplitude S. The resulting correlator due to assumed statistical spatial homogeneity of roughness can be represented as follows (see [34, p. 35]):

$$\overline{S\left(\vec{k}-\frac{\vec{b}}{2},\vec{k}_0-\frac{\vec{b}_0}{2}\right)S^*\left(\vec{k}+\frac{\vec{b}}{2},\vec{k}_0+\frac{\vec{b}_0}{2}\right)} = E(\vec{k},\vec{k}_0;\vec{b})\delta(\vec{b}-\vec{b}_0). \tag{A19}$$

Taking into account that χ is relatively a slow function of $\vec{k}$ and $\vec{k}_0$, one can evaluate the resulting integral in the far field. To do this, one expands the exponent into powers of $\vec{b}$ retaining the lowest order $O(\vec{b})$ terms

$$\vec{\kappa}'\vec{r} - \vec{\kappa}_0'\vec{r}_0 + q_{\kappa_0'}z_0 + q_{\kappa'}z - \left(\vec{\kappa}''\vec{r} - \vec{\kappa}_0''\vec{r}_0 + q_{\kappa_0''}z_0 + q_{\kappa''}z\right) \approx \left(\vec{r}_0 - \vec{r} + \frac{\vec{k}z}{q_k} + \frac{\vec{k}_0 z_0}{q_{k_0}}\right)\vec{b} \tag{A20}$$

and set $\vec{b} = 0$ in all other terms. Note that this assumption imposes certain restrictions on the smoothness of the dependence of function χ on its parameters. Precise conditions of the validity of this approximation require special investigation.

Due to approximation (A20), the integration over $\vec{b}$ produces a δ-function and one finds

$$\overline{|Y(\tau,\omega_D)|^2} = P_{\rm tr}\int\int |D_{\rm tr}(\vec{k}_0)D_{\rm rec}(\vec{k})|^2 E(\vec{k},\vec{k}_0;0) \times \langle|\chi(\delta\tau,\delta\omega,\beta)|^2\rangle\delta\left(\vec{r}_0 - \vec{r} + \frac{\vec{k}z}{q_k} + \frac{\vec{k}_0 z_0}{q_{k_0}}\right) \times \frac{d\vec{k}_0 d\vec{k}}{q_{k_0}q_k}. \tag{A21}$$

In the general case, correlator E contains contribution from both coherent and noncoherent components [34]

$$E(\vec{k},\vec{k}_0;0) = |\overline{V}_{\vec{k}}|^2\delta(\vec{k}-\vec{k}_0) + \frac{1}{4\pi}\frac{\sigma_0(\vec{k},\vec{k}_0)}{q_k q_{k_0}} \tag{A22}$$

where $\overline{V}_k$ is an average reflection coefficient and $\sigma_0(\vec{k},\vec{k}_0)$ is a standard far-field bistatic scattering cross section per unit area (dimensionless values). The average reflection coefficient is associated with the first statistical moment of the scattering amplitude

$$\overline{S(\vec{k},\vec{k}_0)} = \overline{V}_{\vec{k}}\delta(\vec{k}-\vec{k}_0). \tag{A23}$$

After substituting (A22) into (A21), one finds

$$\overline{|Y(\tau,\omega_D)|^2} = \overline{|Y(\tau,\omega_D)|_c^2} + \overline{|Y(\tau,\omega_D)|_{nc}^2} \tag{A24}$$

where contributions from the coherent and noncoherent components are as follows:

$$\overline{|Y(\tau,\omega_D)|_c^2} = P_{\rm tr}\int |D_{\rm tr}(\vec{k})D_{\rm rec}(\vec{k})|^2\langle|\chi(\delta\tau,\delta\omega,\beta)|^2\rangle \times|\overline{V}_{\vec{k}}|^2\ \delta\left(\vec{r}_0 - \vec{r} + \frac{\vec{k}}{q_k}(z+z_0)\right)\frac{d\vec{k}}{q_k^2} \tag{A25}$$

where $\delta\tau$, $\delta\omega$, and β are calculated at $\vec{k} = \vec{k}_0$, and

$$\overline{|Y(\tau,\omega_D)|_{nc}^2} = \frac{P_{\rm tr}}{4\pi}\int\int |D_{\rm tr}(\vec{k}_0)D_{\rm rec}(\vec{k})|^2\langle|\chi(\delta\tau,\delta\omega,\beta)|^2\rangle \times\sigma_0(\vec{k},\vec{k}_0)\delta\left(\vec{r}_0 - \vec{r} + \frac{\vec{k}z}{q_k} + \frac{\vec{k}_0 z_0}{q_{k_0}}\right)\frac{d\vec{k}_0 d\vec{k}}{q_{k_0}^2 q_k^2}. \tag{A26}$$

Let us first perform integration over $\vec{k}$ in the expression for the coherent component. The δ-function results in the following expressions for $\vec{k}$ and q_k:

$$\vec{k} = \frac{\omega_0}{c}\frac{\vec{r}-\vec{r}_0}{R_*},\quad q_k = \frac{\omega_0}{c}\frac{z+z_0}{R_*} \tag{A27}$$

where R_* is given by (6). Calculation of a corresponding Jacobian gives

$$\det \frac{\partial\left(\vec{r}_0 - \vec{r} + \frac{\vec{k}}{q_k}(z+z_0)\right)}{\partial \vec{k}} = \frac{\omega_0^2}{c^2}\frac{(z+z_0)^2}{q_k^4} = \frac{R_*^2}{q_k^2}. \quad \text{(A28)}$$

Then, the following expressions for $\delta\tau$, $\delta\omega_*$, and β_* can be obtained after substituting (A27) into (A15)–(A17):

$$\delta\tau = \beta_*\tau - \frac{\omega_0}{c^2}\frac{z+z_0}{q_k} = \beta_*\tau - \frac{R_*}{c} \quad \text{(A29)}$$

$$\Delta\omega_* = \frac{\omega_0}{c}\frac{(\vec{r}-\vec{r}_0)(\vec{u}^{(0)}-\vec{u}) - (z+z_0)\left(u_z^{(0)}+u_z\right)}{R_*} \quad \text{(A30)}$$

$$\delta\omega_* = \Delta\omega_* - \omega_D \quad \text{(A31)}$$

$$\beta_* = 1 - \frac{\Delta\omega_*}{\omega_0}. \quad \text{(A32)}$$

Using unit vector notations $\vec{m}_*$ and $\vec{n}_*$ from (7) and (8), the expression for $\Delta\omega_*$ in (A30) can be rewritten in a more compact form

$$\Delta\omega_* = \frac{\omega_0}{c}(\vec{m}_*\vec{U}_0 - \vec{n}_*\vec{U}). \quad \text{(A33)}$$

Taking into account (A27), the same unit vector notations can be used for arguments of antenna directivities.

Finally

$$\overline{|Y(\tau,\omega_D)|_c^2} = P_{\rm tr}|D_{\rm tr}(\vec{m}_{*\perp},\omega_0)D_{\rm rec}(\vec{n}_{*\perp},\omega_0)|^2 \times|\chi(\delta\tau,\delta\omega_*,\beta_*)|^2\frac{|\overline{V}(\vec{n}_{*\perp},\omega_0)|^2}{R_*^2}. \quad \text{(A34)}$$

Now, let us consider the noncoherent component (A26). Introducing the integration variable

$$\vec{\rho}_0 = \vec{r}_0 + \frac{\vec{k}_0 z_0}{q_{k_0}} \quad \text{(A35)}$$

instead of $\vec{k}_0$, one finds

$$\vec{k}_0 = \frac{\omega_0}{c}\frac{\vec{\rho}_0-\vec{r}_0}{R_0}, \quad q_{k_0} = \frac{\omega_0}{c}\frac{z_0}{R_0}, \quad R_0 = \sqrt{(\vec{\rho}_0-\vec{r}_0)^2+z_0^2}. \quad \text{(A36)}$$

Similarly, we introduce the integration variable

$$\vec{\rho} = \vec{r} - \frac{\vec{k}z}{q_k} \quad \text{(A37)}$$

instead of $\vec{k}$, which leads to

$$\vec{k} = \frac{\omega_0}{c}\frac{\vec{r}-\vec{\rho}}{R}, \quad q_k = \frac{\omega_0}{c}\frac{z}{R}, \quad R = \sqrt{(\vec{r}-\vec{\rho})^2+z^2}. \quad \text{(A38)}$$

Now, the corresponding Jacobians read

$$\det\frac{\partial\vec{\rho}_0}{\partial\vec{k}_0} = \frac{R_0^2}{q_{k_0}^2}, \quad \det\frac{\partial\vec{\rho}}{\partial\vec{k}} = \frac{R^2}{q_k^2}. \quad \text{(A39)}$$

The δ-function in (A21) turns into $\delta(\vec{\rho}-\vec{\rho}_0)$ so that $\vec{\rho}_0$ in (A36) will be replaced by $\vec{\rho}$. Similar to the above, from (A15)–(A17), one finds

$$\delta\tau = \beta\tau - \frac{R_0+R}{c} \quad \text{(A40)}$$

$$\Delta\omega = \frac{\omega_0}{c}\frac{(\vec{\rho}-\vec{r}_0)\vec{u}^{(0)} - z_0 u_z^{(0)}}{R_0} - \frac{\omega_0}{c}\frac{(\vec{r}-\vec{\rho})\vec{u}+zu_z}{R} \quad \text{(A41)}$$

$$\delta\omega = \Delta\omega - \omega_D \quad \text{(A42)}$$

$$\beta = 1 - \frac{\Delta\omega}{\omega_0}. \quad \text{(A43)}$$

Using (17) and (18), we obtain the expression for $\Delta\omega$ in (A41) in more compact form

$$\Delta\omega = \frac{\omega_0}{c}(\vec{m}\vec{U}_0 - \vec{n}\vec{U}). \quad \text{(A44)}$$

Taking into account (A38), the same unit vector notations can be used for the arguments of antenna directivity functions and σ_0. As a result, one finds

$$\overline{|Y(\tau,\omega_D)|_{nc}^2} = \frac{P_{\rm tr}}{4\pi}\int\int\frac{|D_{\rm tr}(\vec{m}_\perp,\omega_0)D_{\rm rec}(\vec{n}_\perp,\omega_0)|^2}{R_0^2R^2} \times\langle|\chi(\delta\tau,\delta\omega,\beta)|^2\rangle\sigma_0(\vec{n}_\perp,\vec{m}_\perp;\omega_0)d\vec{\rho}. \quad \text{(A45)}$$

It can be shown that introduced here antenna directivities $D_{\rm tr}$ and $D_{\rm rec}$ are related to the standard antenna gain patterns $G_{\rm tr}$ and $G_{\rm rec}$ through the following relationships [4]:

$$|D_{\rm tr}|^2 = \frac{\eta_0}{4\pi}G_{\rm tr} \quad \text{(A46)}$$

$$|D_{\rm rec}|^2 = \frac{\lambda^2}{4\pi}G_{\rm rec} \quad \text{(A47)}$$

where $\eta_0 \approx 120\pi$ Ohms, and λ is a wavelength of the radiation. Taking into account (A46) and (A47), the bistatic radar equation (A45) takes a standard form analogous to [4, eq. (11.185)].

ACKNOWLEDGMENT

The authors would like to thank the anonymous reviewers for their helpful comments.

REFERENCES

[1] V. U. Zavorotny and A. G. Voronovich, "Scattering of GPS signals from the ocean with wind remote sensing application," *IEEE Trans. Geosci. Remote Sens.*, vol. 38, no. 2, pp. 951–964, Mar. 2000.

[2] S. Gleason *et al.*, "Detection and processing of bistatically reflected GPS signals from low Earth orbit for the purpose of ocean remote sensing," *IEEE Trans. Geosci. Remote Sens.*, vol. 43, no. 6, pp. 1229–1241, Jun. 2005.

[3] S. Gleason, S. T. Lowe, and V. U. Zavorotny, "Remote sensing using bistatic GNSS reflections," in *GNSS Applications and Methods*, S. Gleason and D. Gebre-Egziabher, Eds. Boston, MA, USA: Artech House, 2009, pp. 399–436.

[4] F. T. Ulaby and D. G. Long, *Microwave Radar and Radiometric Remote Sensing*. Ann Arbor, MI, USA: Univ. of Michigan Press, 2014, pp. 664–669.

[5] V. U. Zavorotny, S. Gleason, E. Cardellach, and A. Camps, "Tutorial on remote sensing using GNSS bistatic radar of opportunity," *IEEE Geosci. Remote Sens. Mag.*, vol. 2, no. 4, pp. 8–45, Dec. 2014.

[6] G. Foti *et al.*, "Spaceborne GNSS reflectometry for ocean winds: First results from the UK TechDemoSat-1 mission," *Geophys. Res. Lett.*, vol. 42, no. 13, pp. 5435–5441, 2015, doi: 10.1002/2015GL064204.

[7] C. S. Ruf *et al.*, "New ocean winds satellite mission to probe hurricanes and tropical convection," *Bull. Amer. Meteorol. Soc.*, vol. 97, no. 3, pp. 385–395, 2016.

[8] S. Soisuvarn, Z. Jelenak, F. Said, P. S. Chang, and A. Egido, "The GNSS reflectometry response to the ocean surface winds and waves," *IEEE J. Sel. Topics Appl. Earth Observ. Remote Sens.*, vol. 9, no. 10, pp. 4678–4698, Oct. 2016, doi: 10.1109/JSTARS.2016.2602703.
[9] A. K. Fung, C. Zuffada, and C. Y. Hsieh, "Incoherent bistatic scattering from the sea surface at L-band," *IEEE Trans. Geosci. Remote Sens.*, vol. 39, no. 5, pp. 1006–1012, May 2001.
[10] C. Zuffada, A. Fung, J. Parker, M. Okolicanyi, and E. Huang, "Polarization properties of the GPS signal scattered off a wind-driven ocean," *IEEE Trans. Antennas Propag.*, vol. 52, no. 1, pp. 172–188, Jan. 2004.
[11] T. Elfouhaily, D. R. Thompson, and L. Linstrom, "Delay-Doppler analysis of bistatically reflected signals from the ocean surface: Theory and application," *IEEE Trans. Geosci. Remote Sens.*, vol. 40, no. 3, pp. 560–573, Mar. 2002.
[12] J. T. Johnson and T. M. Elfouhaily, "Computation of oceanlike surface thermal emission and bistatic scattering with the reduced local curvature approximation," *IEEE Trans. Geosci. Remote Sens.*, vol. 45, no. 7, pp. 2108–2115, Jul. 2007.
[13] T. M. Elfouhaily and J. T. Johnson, "A new model for rough surface scattering," *IEEE Trans. Geosci. Remote Sens.*, vol. 45, no. 7, pp. 2300–2308, Jul. 2007.
[14] A. G. Voronovich and V. U. Zavorotny, "The transition from weak to strong diffuse radar bistatic scattering from rough ocean surface," *IEEE Trans. Antennas Propag.*, vol. 65, no. 11, pp. 6029–6034, Nov. 2017.
[15] F. T. Ulaby, C. T. Allen, and A. K. Fung, "Method for retrieving the true backscattering coefficient from measurements with a real antenna," *IEEE Trans. Geosci. Remote Sens.*, vol. GRS-21, no. 3, pp. 308–313, Jul. 1983.
[16] R. D. De Roo and F. T. Ulaby, "Bistatic specular scattering from rough dielectric surfaces," *IEEE Trans. Antennas Propag.*, vol. 42, no. 2, pp. 220–231, Feb. 1994.
[17] G. S. Brown, "A theory for near-normal incidence microwave scattering from first-year sea ice," *Radio Sci.*, vol. 17, no. 1, pp. 233–243, Jan./Feb. 1982.
[18] N. R. Peacock and S. W. Laxon, "Sea surface height determination in the Arctic Ocean from ERS altimetry," *J. Geophys. Res.*, vol. 109, no. C7, p. C07001, Jul. 2004, doi: 10.1029/2001JC001026.
[19] G. D. Quartly, "Monitoring and cross-calibration of altimeter σ^0 through dual-frequency backscatter measurements," *J. Atmos. Ocean. Technol.*, vol. 17, no. 9, pp. 1252–1258, 2000.
[20] N. Pierdicca, L. Pulvirenti, F. Ticconi, and M. Brogioni, "Radar bistatic configurations for soil moisture retrieval: A simulation study," *IEEE Trans. Geosci. Remote Sens.*, vol. 46, no. 10, pp. 3252–3264, Oct. 2008.
[21] P. Ferrazzoli, L. Guerriero, N. Pierdicca, and R. Rahmoune, "Forest biomass monitoring with GNSS-R: Theoretical simulations," *Adv. Space Res.*, vol. 47, no. 10, pp. 1823–1832, May 2011.
[22] N. Pierdicca, L. Guerriero, R. Giusto, M. Brogioni, and A. Egido, "SAVERS: A simulator of GNSS reflections from bare and vegetated soils," *IEEE Trans. Geosci. Remote Sens.*, vol. 52, no. 10, pp. 6542–6554, Oct. 2014.
[23] P. Pouliguen, R. Hémon, C. Bourlier, J.-F. Damiens, and J. Saillard, "Analytical formulae for radar cross section of flat plates in near field and normal incidence," *Prog. Electromagn. Res. B*, vol. 9, pp. 263–279, 2008. [Online]. Available: http://www.jpier.org/PIER/pier.php?volume=09
[24] D. G. Falconer, "Extrapolation of near-field RCS measurements to the far zone," *IEEE Trans. Antennas Propag.*, vol. AP-36, no. 6, pp. 822–829, Jun. 1988.
[25] *IEEE Recommended Practice for Radar Cross-Section Test Procedures*, IEEE Standard 1502, 2007, p. 2.
[26] A. Alonso-Arroyo, V. U. Zavorotny, and A. Camps, "Sea ice detection using U.K. TDS-1 GNSS-R data," *IEEE Trans. Geosci. Remote Sens.*, vol. 55, no. 9, pp. 4989–5001, Sep. 2017.
[27] A. Napolitano, *Generalizations of Cyclostationary Signal Processing: Spectral Analysis and Applications*. Hoboken, NJ, USA: Wiley, 2012.
[28] A. Napolitano and I. Perna, "Cyclic spectral analysis of the GPS signal," *Digit. Signal Process.*, vol. 33, pp. 13–33, Oct. 2014.
[29] E. Cardellach *et al.*, "Consolidating the precision of interferometric GNSS-R ocean altimetry using airborne experimental data," *IEEE Trans. Geosci. Remote Sens.*, vol. 52, no. 8, pp. 4992–5004, Aug. 2014.
[30] M. P. Clarizia, C. Ruf, P. Cipollini, and C. Zuffada, "First spaceborne observation of sea surface height using GPS-reflectometry," *Geophys. Res. Lett.*, vol. 43, no. 2, pp. 767–774, 2016.
[31] C. Hu, C. Benson, C. Rizos, and L. Qiao, "Single-pass sub-meter space-based GNSS-R ice altimetry: Results from TDS-1," *IEEE J. Sel. Topics Appl. Earth Observ. Remote Sens.*, vol. 10, no. 8, pp. 3782–3788, Aug. 2017, doi: 10.1109/JSTARS.2017.2690917.
[32] J. L. Garrison, S. J. Katzberg, and M. I. Hill, "Effect of sea roughness on bistatically scattered range coded signals from the global positioning system," *Geophys. Res. Lett.*, vol. 25, no. 13, pp. 2257–2260, Jul. 1998.
[33] M. Martín-Neira, S. D'Addio, C. Buck, N. Floury, and R. Prieto-Cerdeira, "The PARIS ocean altimeter in-orbit demonstrator," *IEEE Trans. Geosci. Remote Sens.*, vol. 49, no. 6, pp. 2209–2237, Jun. 2011.
[34] A. G. Voronovich, *Wave Scattering from Rough Surfaces*, 2nd ed. Berlin, Germany: Springer, 1999.
[35] A. G. Voronovich and V. U. Zavorotny, "Full-polarization modeling of monostatic and bistatic radar scattering from a rough sea surface," *IEEE Trans. Antennas Propag.*, vol. 62, no. 3, pp. 1362–1371, Mar. 2014.
[36] T. Elfouhaily, B. Chapron, K. Katsaros, and D. Vandemark, "A unified directional spectrum for long and short wind-driven waves," *J. Geophys. Res.*, vol. 102, no. C7, pp. 15781–15796, 1997.
[37] *CYGNSS Project*, document 148-0123, Space Physics Research Laboratory, Univ. Michigan, Jan. 2014, pp. 1–24.
[38] S. Gleason, C. S. Ruf, M. P. Clarizia, and A. J. O'Brien, "Calibration and unwrapping of the normalized scattering cross section for the Cyclone Global Navigation Satellite System," *IEEE Trans. Geosci. Remote Sens.*, vol. 54, no. 5, pp. 2495–2509, May 2016.
[39] M. P. Clarizia and C. S. Ruf, "Wind speed retrieval algorithm for the Cyclone Global Navigation Satellite System (CYGNSS) mission," *IEEE Trans. Geosci. Remote Sens.*, vol. 54, no. 8, pp. 4419–4432, Aug. 2016.
[40] F. Saïd, S. Soisuvarn, Z. Jelenak, and P. S. Chang, "Performance assessment of simulated CYGNSS measurements in the tropical cyclone environment," *IEEE J. Sel. Topics Appl. Earth Observ. Remote Sens.*, vol. 9, no. 10, pp. 4709–4719, Oct. 2016.

Alexander G. Voronovich received the M.Sc. degree in physics and the Ph.D. degree in theoretical and mathematical physics from the Moscow Institute of Physics and Technology, Moscow, Russia, in 1972 and 1975, respectively, and the Dr.Sc. degree in theoretical and mathematical physics from the Acoustical Institute, Moscow, in 1988.

From 1975 to 1979, he was a Junior Research Scientist with the Acoustical Institute. In 1980, he joined the P. P. Shirshov Institute of Oceanology, Moscow, as a Senior Research Scientist, and became a Professor of physics with the Moscow Institute of Physics and Technology, in 1991. From 1989 to 1993, he was the Head of the Laboratory of Acoustical Waves Propagation in the Ocean, P. P. Shirshov Institute of Oceanology. He is currently an Oceanographer with the Earth System Research Laboratory, National Oceanic and Atmospheric Administration, Boulder, CO, USA. His research interests include wave scattering from rough surfaces, ocean acoustics, geophysical hydrodynamics, internal waves, and linear and nonlinear theory of wave propagation.

Dr. Voronovich is a fellow of the Acoustical Society of America.

Valery U. Zavorotny (M'01–SM'03–F'10) received the M.Sc. degree in radio physics from Gorky State University, Gorky, Russia, in 1971, and the Ph.D. degree in physics and mathematics from the Institute of Atmospheric Physics, USSR Academy of Sciences, Moscow, Russia, in 1979.

From 1971 to 1990, he was with the Institute of Atmospheric Physics, USSR Academy of Sciences. In 1990, he joined the Lebedev Physical Institute, Moscow. He is currently a Physicist with the Earth System Research Laboratory, National Oceanic and Atmospheric Administration, Boulder, CO, USA. He is a member of the NASA CYGNSS Mission Science Team. His research interests include the theory of wave scattering from rough surfaces, ocean and land remote sensing applications using radar, and global navigation satellite system reflection techniques.

Dr. Zavorotny is a member of the American Geophysical Union and Commission F of the U.S. National Committee of URSI. He is a Distinguished Lecturer of the Geoscience and Remote Sensing Society. He was a recipient of the 2014 Prince Sultan Bin Abdulaziz International Creativity Prize for Water (jointly with K. Larson, E. Small, and J. Braun).